Journal of Thermal Analysis and Calorimetry
https://doi.org/10.1007/s10973-023-12810-0

Synthesize of exfoliated poly-methylmethacrylate/organomontmorillonite nanocomposites by in situ polymerization: structural study, thermal properties and application for removal of azo dye pollutant

Smail Terchi[1,2] · Samir Hamrit[3,4] · Naziha Ladjal[5] · Khaldoun Bachari[6] · Hafsia Ben Rhaiem[7]

Received: 18 June 2023 / Accepted: 3 December 2023

Abstract
This paper reports the synthesis of exfoliated structure of Poly-methylmethacrylate/organomontmorillonite nanocomposites by in situ polymerization of Methylmethacrylate monomer as a cost-effective adsorbent for ultrahigh removal of azo dye pollutant from aqueous media. The obtained nanocomposites with different organoclay loading (1–7 mass%) were characterized by XRD, FTIR, DTA, TGA, TEM and SEM. In the XRD results, the observation of small pick shoulders (d_{001}) and almost no reflection in the X-ray diffractograms indicated, respectively, the establishment of intercalated/exfoliated structures and major exfoliation of OMMT clay into polymer. This observation was supported by TEM microscopy. TGA results revealed improved thermal properties in comparison with the pure polymer. Adsorption parameters such as pH-value, contact time and initial dye concentration were investigated to assess optimum adsorption activity. The adsorption experiments showed that the equilibrium time of adsorption was reached very rapidly. According to the kinetic study, the adsorption process followed pseudo-second-order model. The adsorption capacity is unaffected by variation of solution pH. The high maximum adsorption capacity of PMMA/OMT nanocomposite toward dye was found to be 309.6 mg g^{-1}. Langmuir isotherm was more suitable model to describe the adsorption of dye than Freundlich and Dubinin–Radushkevich models. Thermodynamic study showed that the removal of the azo dye from aqueous solution by PMMA/OMT nanocomposite is endothermic nature, spontaneous and physisorption process. Under three adsorption–desorption cycles, PMMA/OMT nanocomposite had good re-adsorption effect. Thus, PMMA/OMT nanocomposite can be an efficient and recyclable adsorbent for azo dyes.

Keywords Clay/polymers nanocomposites · Thermal analysis · In situ polymerization · Wastewater treatment · Thermodynamic study · Azo textile dyes

✉ Smail Terchi
smail.terchi@univ-msila.dz

[1] Département de Chimie, Faculté des Sciences, Université de M'sila, M'sila, Algeria

[2] Laboratoire Matériaux et Energies Renouvelabes, Université Mohamed Boudiaf M'Sila, 28000 M'sila, Algeria

[3] Département de Physique, Faculté des Sciences, Université de M'sila, M'sila, Algeria

[4] Laboratoire de Physique des Matériaux et ses Applications, Université Mohamed Boudiaf M'sila, M'sila, Algeria

[5] École Normale Supérieure de Bou Saada, Bou Saada, Algeria

[6] Centre de Recherche Scientifique et Technique en Analyses Physico-Chimiques (CRAPC), BP 248, 16004 Bou Ismaïl, Algeria

[7] Laboratoire de Physique des Matériaux Lamellaires et Nanomatériaux Hybrides, Faculté des Sciences de Bizerte, Université de Carthage, Tunis, Tunisia

Published online: 13 January 2024

Introduction

Recently, the Poly Methyl Methacrylate polymers (PMMA) have received a lot of attention due to their toughness, lightweight, and lower density in comparison with glass [1, 2]. PMMA is a bio-compatible polymer with wide application in tooth restoration, protective eye wear, airplane windows, room walls, ornaments, luxury goods, and large aquarium panels [3]. It has excellent transparency, high elastic modulus, well flexibility, high strength, and excellent dimension stability but has a rather high melt viscosity (> 104 Pa s). It has also been reported that the PMMA cannot meet the present requirements due to their poor heat resistance and mechanical properties such as wear and abrasion which are relatively low and independent of molecular weight. In last years, much interest of academia and industrial chemists has been paid to polymer–clay nanocomposite, because the efficient incorporation of clay into a polymer matrix can significantly improve the thermal stability and mechanical properties of neat polymer without significantly reducing optical clarity [4, 5].

It has been reported that PMMA/montmorillonite clay nanocomposites are prepared by various methods such as in situ polymerization, solution blending and melt blending [6–8]. Two different nanostructures have been identified in these nanocomposites: intercalated and exfoliated nanostructures[9, 10]. Exfoliated nanostructures are preferable to intercalated nanostructures due to the strong synergy between the polymer matrix and the silicate layers[11]. Among these methods of preparation, the in situ polymerization is a promising method for preparation of exfoliated nanocomposites [10].

Many researchers have reported the use of various organic modifiers of montmorillonite such as surfactants, Gemini surfactants and silanes to achieve better compatibility and dispersion of clay platelets in the polymer matrix [12–14]. Prado and Bartoli [10] have used emulsion polymerization assisted by sonication for the preparation of exfoliated/intercalated and intercalated morphologies of PMMA/OMMT nanocomposites. However, achieving the total exfoliation of clays in polymers matrix remains a challenging task and is still constrained in its realization.

Alexandros et al. [2] prepared poly methyl methacrylate/organo modified montmorillonite nanocomposites by in situ bulk polymerization method. The structures and morphologies of the prepared nanocomposites results have indicated that exfoliation is more possible to take place in case of nanocomposites with low amounts of organo modified montmorillonite. However, the thermal stability of nanocomposites was improved by increasing the amounts of OMMT.

In the first aim of this work, a try was made to prepare exfoliated structure of PMMA/OMMT nanocomposites by in situ polymerization in the presence of organo modified local (Algerian) montmorillonite with different amounts (1–7%) knowing that the improvement in thermal stability of the nanocomposites is mainly due to exfoliated structure, in which the interaction between the clay and the polymer is maximized, the clay surface area available for the polymer matrix is larger [15]. So, the thermal stability improvement of prepared nanocomposites is investigated.

In the other hand, it is known that the textile industry is a major cause of water pollution because of the important volumes of extensively contaminated wastewater that it discharges into the environment [16]. The textile dyes are among of hazardous chemical compounds presented in the textile effluent which are toxic to aquatic and non-aquatic organisms and can cause cancer for humans [17, 18]. As a result, the direct discharge of textile effluent into water causes ecosystem and health problems [19, 20]. Azo dyes are the most often used dyes in the industrial textile.

(Approximately 70% of all dyes), Since they are high soluble in the water, the azo group (–N=N–) is stable [21, 22]. Complex aromatic structures in azo dyes (–N=N– groups) prevent biodegradation, allowing them to survive in the environment for lengthy periods of time [23]. Given the environmental effect caused by dye pollution, effective methods should be used to treat textile wastewater polluted by coloring agents, such as azo dyes, before their release into the environment. Among several physical and chemical techniques used to removal of azo dye effluents such as coagulation–flocculation [24], electrocoagulation [25, 26], photocatalysis [27–29], membrane filtration [30, 31], and several other techniques, adsorption techniques are widely used due to their simplicity, low cost and ease of process. To remove dyes from aqueous environments, many different types of adsorbents have been used, including activated carbon [32–34], agricultural and industrial wastes [35], biosorbents [36, 37], clays [31, 38–41] and clay-polymer nanocomposites [42–44], but the use of clay/PMMA nanocomposite as adsorbent for dyes is not investigated yet. The novelty of our study lies in utilizing PMMA/Organo-Algerian montmorillonite as an eco-friendly and cost-efficient adsorbent for the removal of the azo dye (Nylosan Red dye) from aqueous solutions. Moreover, we investigate the reusability of the nanocomposite adsorbent to further minimize the cost of treating polluted water. This comprehensive exploration aims to contribute to both the advancement of polymer nanocomposites and the effective treatment of wastewater contaminated with azo dyes, addressing critical environmental and health concerns.

Experimental

Materials

Methyl methacrylate monomer (MMA) with density of 0.936 g cm^{-3} and Benzoyl peroxide initiator (BPI) was purchased from Alfa Aesar, the MMA was purified by distillation under reduced pressure, Octadecylamine, Dichloromethane and Hexane were purchased from Sigma Aldrich, Methanol from Biochem. The azo dye (Nylosan Red N-2RBL) was purchased from Varian, with a molecular weight of 587.97 g mol^{-1} and solubility in water of 80 g L^{-1} [39], and its chemical structure is depicted in Fig. 1. Pristine MMT with a cation exchange capacity (CEC) of 95 meq/100 g of clay was procured from Maghnia plant, west of Algeria [45].

Organomontmorillonite synthesize

Prior to the modification of clay and its later use in polymerization, impurities must be separated from natural MMT. The purification of available natural montmorillonite (MMT) was carried out in the following manner:

In order to eliminate the organic impurities, the montmorillonite was first rinsed with distilled water and hydrogen peroxide (30%) using a stirring process for 48 h. The mixture was then rinsed in distilled water at room temperature numerous times and dried in the oven at 50 °C for 7 days. The recovered montmorillonite was added into solution of NaCl with 1CEC of clay and agitated at 70 °C for 8 h. The suspension was rinsed many times by centrifugation method with distilled water until negative test of Cl^- ions that was detected with $AgNO_3$ solution test. The recovered clay was dried at 80 °C for one day in the vacuum oven.

The obtained product was crushed and sieved (< 90 µm). After that, the montmorillonite suspensions were placed in centrifuge tubes and then suctioned out with a syringe to recover the montmorillonite fraction with a particles size < 2 µm. The discarded materials were gathered and stored for future use. To gather a sufficient amount of fractionated montmorillonite, the operation was repeated many times for each sampling.

The recovered suspension was then dried at 80 °C and milled with a mortar. The obtained fractionated clay was designed as FNaMMT [45]. The organomontmorillonite was synthesized by cationic exchange mechanism between the fractionated montmorillonite and the alkyl ammonium (ODA) in aqueous media. 30 g of FNaMMT were added into 500 mL of hot water (80 °C) and agitated for 1 h. 7.68 g of ODA was dissolved in a mixture of distilled water and HCl (36%) at 80 °C for 3 h with agitating. The obtained mixture was left to itself at ambient temperature without agitating for one day. The product was washed several times with hot distilled water (80 °C) until negative test of Cl^- anions using $AgNO_3$ tests. The precipitate was then dried to obtain organomontmorillonite (OMMT).

Synthesize of PMMA/OMMT nanocomposites

According to the typical method for synthesis of PMMA/OMMT nanocomposites with a 1% of clay loading, 0.1 g of OMMT was first dispersed into 30 mL of distilled toluene and magnetically stirred for an entire night at room temperature.

This suspension was mixed with 9.9 g of MMA monomer and 0.097 g of benzoyl peroxide initiator (BPI) and

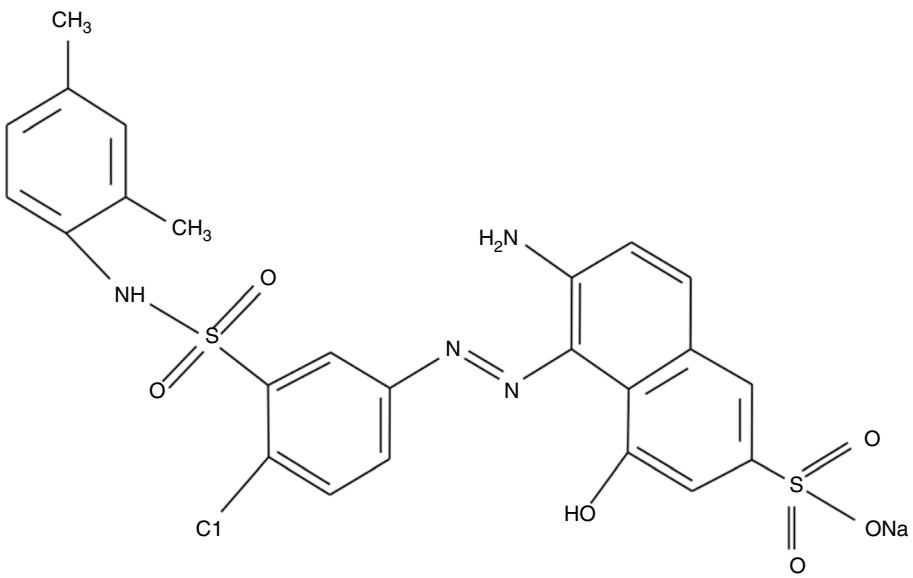

Fig. 1 Chemical structure of the anionic azo dye (Nylosan Red N-2RBL)

magnetically stirred for 5 h 75 °C in inert atmosphere. The obtained product was separated after dissolution in n-Hexane and precipitated in methanol.

The obtained PMMA/OMMT nanocomposites were dried at 80 ° for 5 h.

Adsorption of Nylosan Red dye experiments

The adsorption of the azo dye (Nylosan Red) onto PMMA/(7 mass% of OMMT) nanocomposite sample was studied in batch adsorption experiments. In this study, the parameters of pH of the solution, contact time, and dye concentration were examined.

The kinetic study was carried out at 20 °C. Several solutions of NR dye of 25 mL and initial concentrations of 25, 50 and 100 mg L^{-1} were prepared. They were combined with 20 mg of nanocomposite in closed agitated flasks (300 rpm). The residual dye concentration in each flask was measured after increasing contact time (between 2.5 and 180 min). Batch pH studies were carried out by addition of 20 mg of the nanocomposite into 25 mL of each dye solution (200 mg L^{-1}) in closed agitated flasks (300 rpm) for 18 hat 20 °C; the pH values were ranging from 2 to 12. The pH of the solutions was adjusted with NaOH or solution HCl by using a pH meter.

The equilibrium adsorption experiments were carried out in closed flasks containing 20 mg of nanocomposite and 25 mL of dye solution with initial concentrations ranging from 20 to 600 mg L^{-1} for 18 h at 20 °C.

The thermodynamic adsorption experiments were carried out in closed flasks containing 20 mg of nanocomposite and 25 mL of azo dye solution of initial concentration 50 mg L^{-1} for 2 h at different temperatures 25 °C, 35 °C and 45 °C.

After separation, the dye equilibrium concentrations (q_e) were measured by spectrophotometry (Shimadzu UV-2101PC) at 502 nm. The NR equilibrium concentrations were determined using Eq. (1) after calibration with a high regression coefficient value of 0.999:

$$C_e = (\text{Abs} - 0.097)/0.01 \quad (1)$$

The difference between the initial and equilibrium NR concentrations was used to calculate the quantity of adsorbed NR (q_e):

$$q_e = \left(C_i - C_e\right) \cdot V/m \quad (2)$$

Where q_e is the quantity of adsorbed dye per unit mass of nanocomposite (mg g^{-1}), C_i and C_e: are the initial and equilibrium azo dye concentrations (mg L^{-1}), respectively, m: is the mass of utilized nanocomposite, and V: is the volume of dye solution (25 mL). The adsorption efficiency of the azo dye was calculated by following equation:

$$R(\%) = \left[\left(C_i - C_e\right)/C_i\right] \times 100 \quad (3)$$

Characterizations

X-ray diffraction patterns were followed up by a BRUKER diffractometer with CuK_α radiation source ($\lambda = 1.54$ Å). The basal spacing (d_{001}) of the montmorillonite layers was calculated using Bragg's equation Eq. (4):

$$2d \cdot \sin\theta_{max} = n\lambda \quad (4)$$

All scanning was done in 2θ range between 1 and 10°.

The Infrared spectroscopy (FTIR) measurements were recorded on a Shimadzu spectrophotometer (FTIR-8300), using the KBr compacted disc technique.

Thermal gravimetric (TG) and deferential thermal analysis (DTA) analysis were performed on DW5470H63 STA analyzer under nitrogen atmosphere, and heating from room temperature to 700 °C, at the rate of 10 °C min^{-1}.

The scanning electronic microscopy (SEM) images were performed with a field emission scanning electron microscopy (SEM, Quanta 250).

The transmission electronic microscopy (TEM) images of the nanocomposites were obtained using a Philips CM20 instrument operating at 200 kV equipped with Energy Dispersive X-ray Spectrometer (EDS).

The Point of zero charge (pH_{pzc}) of selected nanocomposite for adsorption was determined by NaCl salt addition method.

Results and discussion

SEM results

SEM was used to examine the morphology of organomontmorillonite (OMMT) and the fractured surfaces of Charpy impact samples to evaluate the dispersion of OMMT in PMMA matrix, and the SEM microphotographs are shown in Fig. 2.

Figure 2a shows an excellent dispersion of octadecylammonium in the montmorillonite. Figure 2b–e reveals that OMMT microsheets disperse homogeneously in PMMA matrix although they do not show an exfoliated-intercalated nanostructure. The interfaces between OMMT sheets and PMMA matrix are blurry, which indicates that the interfacial interaction between PMMA matrix and OMMT microsheets is improved mainly due to the modification of MMT by octadecylammonium. PMMA/OMMT nanocomposites are anticipated to significantly improve the mechanical and flame retardant properties of polymer due to the well-dispersed

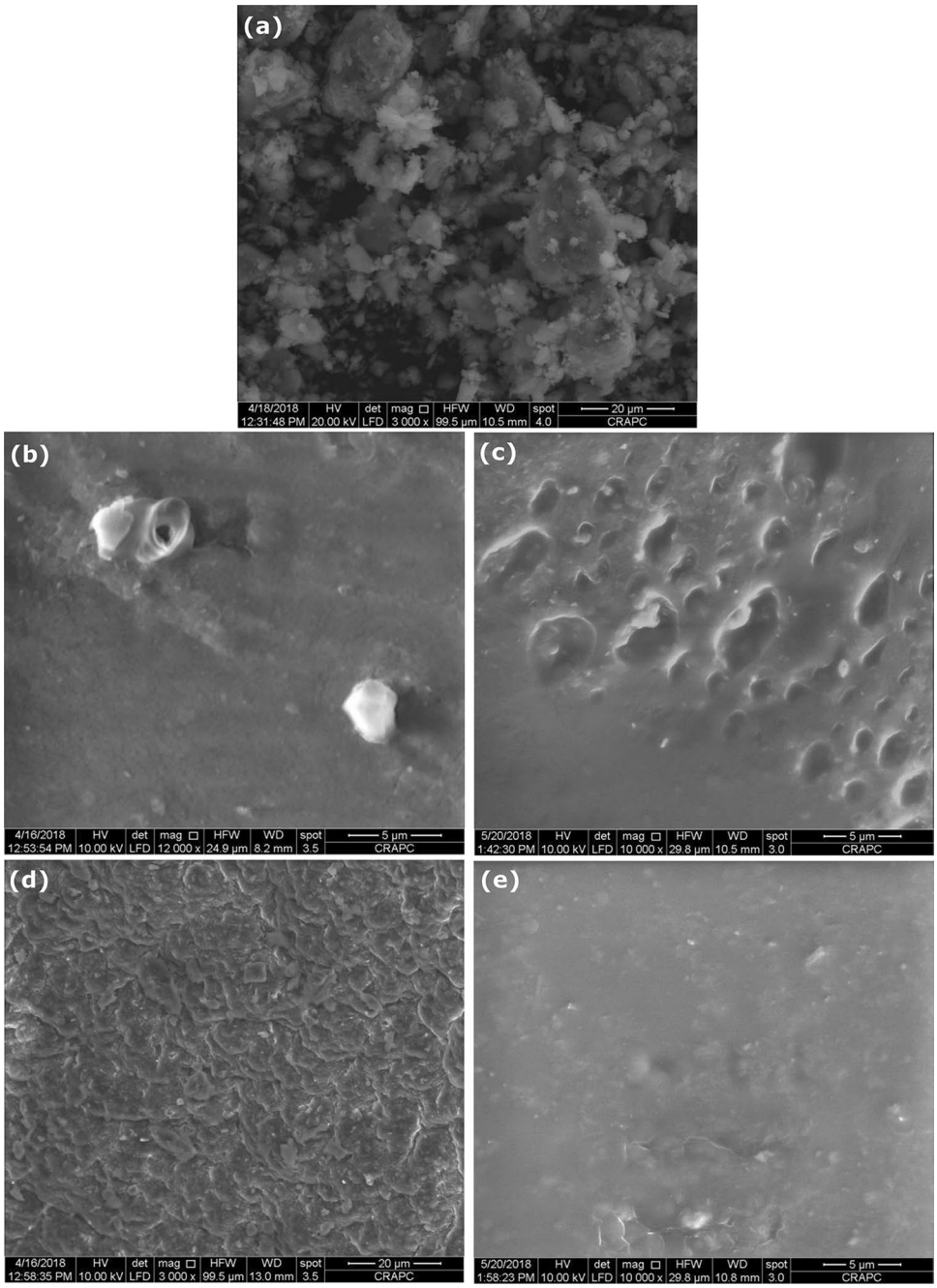

Fig. 2 SEM images illustrating PMMA/OMMT nanocomposites with various OMMT loadings: **a** 0%, **b** 1%, **c** 3%, **d** 5% and **e** 7%

organoclay microsheets and increased interfacial contact between PMMA matrix and organoclay microsheets [46].

XRD results

Due to its high interlayer spacing, the virgin Algerian montmorillonite was chosen for this study. According to the JCPDS card (No. 00-046-1045), the XRD pattern in Fig. 3a shows a typical reflection of fractionated organoclay powder OMMT at $2\theta = 4.22°$ (d-value = 20.92 Å). This increase in d-value, relatively to the pristine sodic montmorillonite (15.24 Å) can be explained by the incorporation of an important amount of octadecylammonium inside the interlayer space [45]. The neat PMMA (0%) sample without organoclay (Fig. 3b) showed no reflection in 2θ range, the amorphous phase of the polymer is responsible for this property.

The XRD patterns of the PMMA-ODA samples containing 1% and 5% mass of OMMT showed a shoulders at $2\theta = 2.46°$ (d-value = 35.07 Å); these shoulders could be associated with an intercalation structure (Fig. 3c–e). Whereas PMMA/OMMT samples containing 3% and 7% mass of OMMT showed light shoulders (Fig. 3d–f). Whether these shoulders were a real reflection or not, it seems that well clay dispersions were produced in PMMA matrix, this probably due to certain exfoliated and intercalated structures.

Furthermore, during the polymerization of these nanocomposites with vigorous stirring, the (MMA monomer-solvent) mixture inserted in clay interlayers and the growth of polymer chain pushed the clay layers apart to the point where the d-value could not be seen with XRD ($2\theta > 1°$).

Some studies Kowalczyk et al. [47], Valandro et al. [48], Tsai et al. [49], Morgan et al. [50] reported that XRD is used to determine the basal spacing (d_{001})-value in intercalated structure. However, it is not always able to identify exfoliated nanocomposite with no XRD reflections or detect low clay loadings (less than 5%).

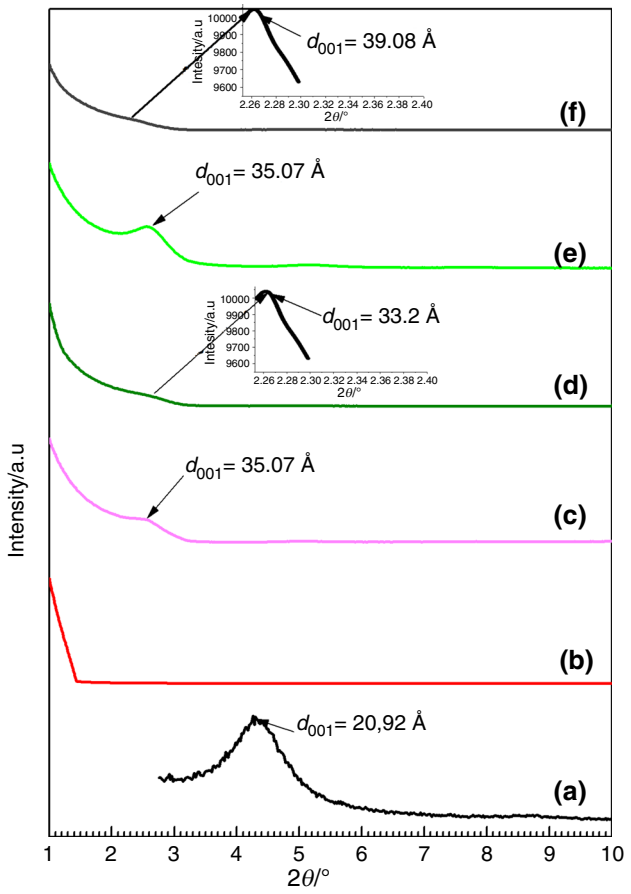

Fig. 3 XRD patterns of OMMT (**a**) and PMMA/OMMT nanocomposites with various OMMT contents: **b** 0%, **c** 1%, **d** 3%, **e** 5% and **f** 7%

Consequently, the XRD technique is useful for identifying the clay's dispersion state in the polymer matrix, it does not give a full picture of the extent of intercalation and exfoliation of organo modified clays.

TEM results

A complementary technique to XRD analysis, transmission electron microscopy (TEM) provides further details on the dispersion state of clay in the polymer matrix.

The TEM analyses were only carried out for the PMMA/ODA1% which presented shoulder reflection and PMMA-OMMT7% where almost no reflection is observed in the XRD patterns. Figure 4a shows TEM image of PMMA/OMMT1% sample that revealed good dispersed and disoriented clay platelets, exfoliated layers and clay layer stacks are also depicted in the figure. However, Fig. 4b shows an intercalating tactoids consisting of a stacking of many platelets presenting in the polymer.

Therefore, TEM pictures of the PMMA/OMMT1% nanocomposite displayed a mixed morphology of intercalated and exfoliated structures, or partially exfoliated nanocomposite.

On the other hand, Fig. 4c shows TEM image of PMMA/OMMT7% sample and revealed clear exfoliated clay platelets.

TG and DTA results

Figure 5a–e illustrates thermogravimetric analysis of prepared pristine PMMA 0%and PMMA/OMMT (1, 3, 5 and 7%) nanocomposites; the analysis was carried out in nitrogen atmosphere to determine the mass loss caused by thermal degradation. Figure 5a shows that the degradation of pure PMMA occurs through two main reaction stages; the first stage at temperatures ranging from 160 to 240 °C, which can be split into two steps; decomposition of weak head-to-head links and impurities, and decomposition of the ends of chain polymer at about 270 °C. The second stage at temperatures ranging between 300 and 450 °C, which could be attributed to random scission of the polymer chains. Our results were in agreement with the finding reported by Hirata et al. [51]. McNeill et al. [52] reported a study of thermal degradation of PMMA in inert atmosphere and have been found two temperatures of 285 °C and 380 °C for both two degradation steps of PMMA which, respectively, were attributed to the unzipping and random scission reactions.

The temperatures at 5% ($T_{5\%}$) and 50% ($T_{50\%}$) of mass loss, T_{max} and the T_g temperatures are summarized in Table 1.

The $T_{5\%}$ of mass loss for pristine PMMA is around 180 °C; however, at the same temperature, the percentage (%) of mass loss of the nanocomposites at various OMMT loading (1, 3, 5 and 7%) are gradually decreasing (4.5, 3.5,

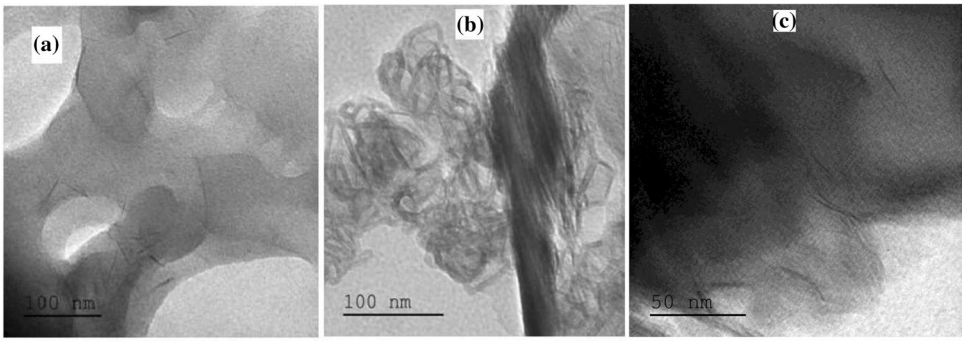

Fig. 4 TEM images of PMMA/OMMT with: 1% OMMT loading **a** partial exfoliation and **b** partial intercalation, 7% OMMT loading **c** exfoliation.

2.8 and 2.7%), respectively. It can be also observed from Table 1 that the temperature at 5% degradation $T_{5\%}$ is increasing slightly as the OMMT loading increases (exception was noted for 7% OMMT loading). The mass loss at 5% is probably caused by the degradation of both nanofillers (OMMT) and weak linkage of PMMA.

Therefore, the clay's barrier property, confinement, and cross-linking function contribute simultaneously to the enhancement of the thermal property.

The temperature at 50% of mass loss of the PMMA is approximately 326 °C. At this temperature, the mass loss of the various nanocomposites was significantly decreased. The $T_{50\%}$ for PMMA 1% and 3% of OMMT loading was significantly increased from 326 °C to 379 and 382 °C, respectively. Meanwhile, it decreases for PMMA 7% sample. The temperature at a maximum rate of degradation T_{max} determined by the second peak of the first derivative reveals a significant increase in temperature when 1% of OMMT was added (≈ 17 °C higher). The temperature gradient was jumping to 394 °C when 3% of OMMT was loaded (≈ 34 °C higher). Consequently, PMMA/OMMT nanocomposites showed an improvement in thermal stability when is compared to the virgin polymer, which is consistent with literature data [6].

In order to investigate the mobility of the PMMA chain, the T_g (glass transition temperature) was determined using the DTA analysis. The DTA results of pristine PMMA and PMMA/OMMT nanocomposites are also shown in Table 1. T_g rises from 109 to 122 °C when 1% of OMMT content was added (≈ 14 °C higher). At 3% of OMMT loading, the T_g increases slightly (≈ 6 °C) as compared to the virgin polymer. At 7% of OMMT content, the T_g increases and reaches 129 °C (≈ 21 °C higher). This can be explained when OMMT content increases, the molecular chains of PMMA restricted by OMMT sheets increase in the nanocomposites and the cross-linking points and density also increase; this promotes the enhancement in the temperature of thermal decomposition and T_g (glass transition temperature), thus, an enhancement in the thermal stability of the nanocomposites [6].

FTIR results

The FTIR spectra of fractionated (FNaMMT) and the correspondent organoclay (OMMT) are shown in Fig. 6a and b, respectively. As shown in Fig. 6a, transmittance peaks of FNaMMT show O–H stretching vibrations of silicate layers at 3638 cm^{-1} and bending vibrations of O–H groups at 1641 cm^{-1}, the Si–O stretching vibration is observed at 1100 cm^{-1}. The Si–O–Al bending vibrations are detected in the range of 500–700 cm^{-1}.The band located at 798 cm^{-1}may be due to the amorphous silica presented in the montmorillonitic clay [53].

In Fig. 6b the peaks at 2921 and 2862 cm^{-1}correspond, respectively, to asymmetric and symmetric C–H stretching vibrations of alkylic group of the ODA surfactant [54]. The peaks at 1500 cm^{-1} correspond to the N–H bending of haloalkylic group (CH_3–Cl), due to the intercalation of ODA surfactant [55].

Figure 7 shows FTIR spectra of pure PMMA (Fig. 7a) and PMMA/OMMT nanocomposites (Fig. 7b–e) samples. In Fig. 7a, the absorption bands at 2950 and 2845 cm^{-1} are attributed to CH_2 stretching, and the bands at 1465 and 756 cm^{-1} are assigned, respectively, to the bending and rocking vibrations of CH_2 of PMMA chains. The band located at 1733 cm^{-1} corresponds to the stretching vibrations of C=O group of pristine PMMA. After the preparation of PMMA/OMMT nanocomposites, it can be observed that after incorporation of OMMT in PMMA matrix, the stretching vibration of the C=O group appearing at 1733 cm^{-1} for pristine PMMA was shifted to lower values (1730 cm^{-1}) Fig. 7b–e [56]. The peak appeared at 1627 cm^{-1} is attributed to the hydrogen-bonded carbonyl groups [55]. Furthermore, the absorption peak at 3638 cm^{-1} corresponds to OH stretching presented in OMMT sample (Fig. 6a) and shifts to a lower value 3628 cm^{-1}. As a result, there is an interaction between molecular chains of PMMA and OMMT. Thus, the FTIR analysis has clearly demonstrated that the OMMT has been successfully incorporated into the polymer matrix.

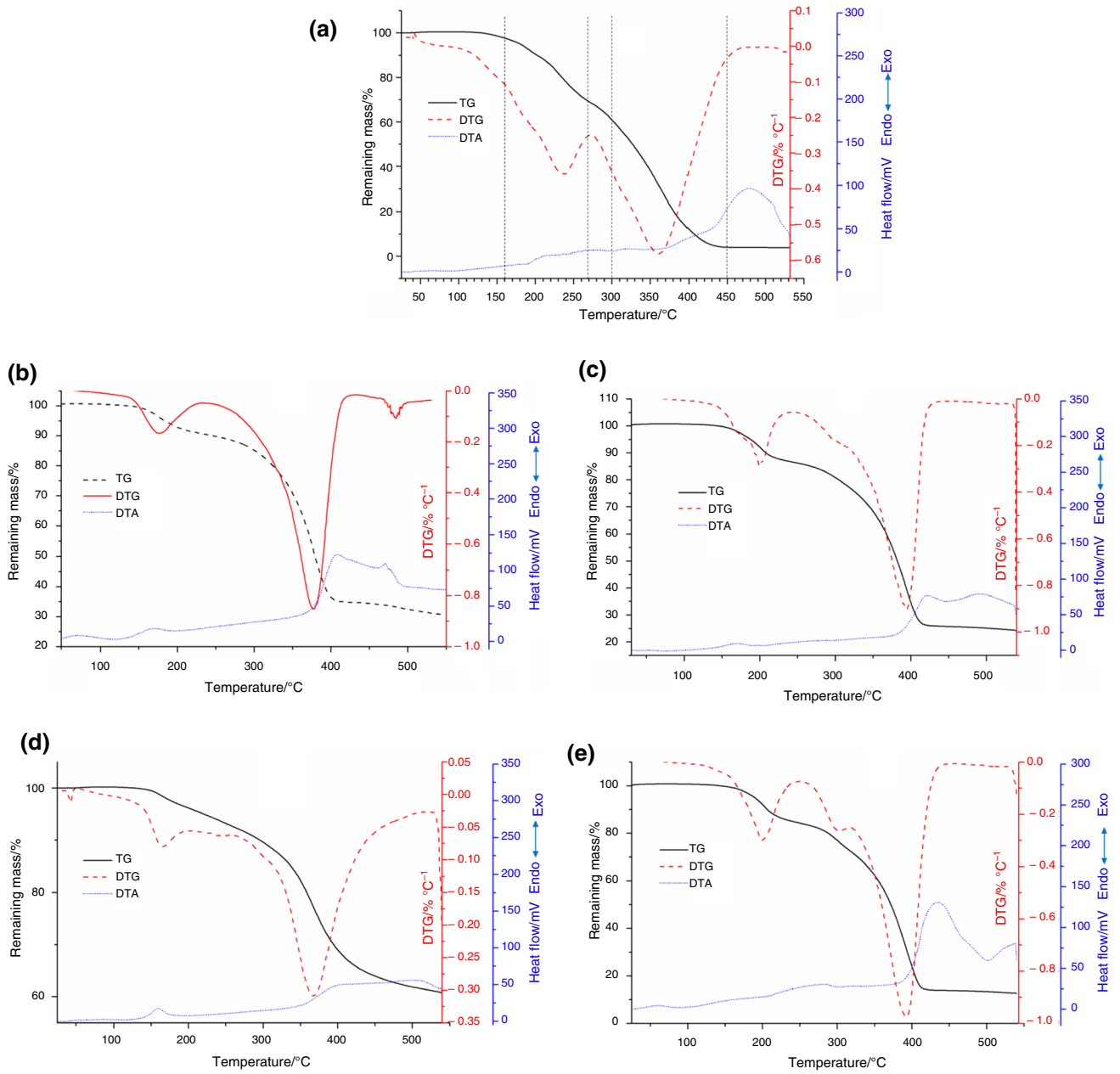

Fig. 5 TG, DTG and DTA curves of PMMA/OMMT nanocomposites with different OMMT loading: **a** 0%, **b** 1%, **c** 3%, **d** 5% and **e** 7%

Table 1 TG and DTA results of PMMA and PMMA/OMMT nanocomposites

% OMMT	% of degradation $T=180$ °C	% of degradation $T=201$ °C	% of degradation $T=326$ °C	$T_{5\%}$/°C	$T_{50\%}$/°C	T_{max}/°C	T_g/°C
0%	5	10	50	180	326	360	109
1%	4.5	7.4	20.5	184	379	377	122
3%	3,5	7.2	24.23	189	382	394	114
5%	2,8	4.1	13.25	207	–	368	180
7%	2,7	8.2	29.46	189	371	392	129

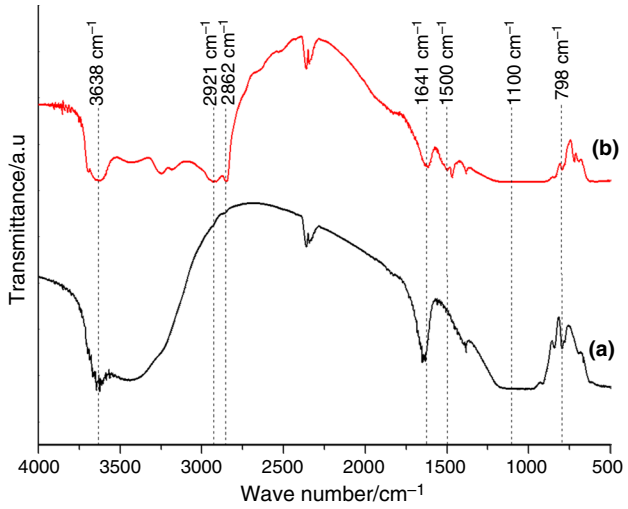

Fig. 6 FTIR spectra of: **a** FNaMMT and **b** OMMT

pH at point zero charge

The zero charges point (pH_{pzc}) is a critical parameter which indicates a pH-value where the surface charge on the adsorbent has a zero charge. Thereby, the surface charge of solid is negative if $pH > pH_{pzc}$ and positive if $pH < pH_{pzc}$.

The pH of suspension of the selected sample for adsorption (0.15 g of PMMA/OMMT, 7 mass%) and NaCl aqueous solution (50 mL, 0.01 mol L^{-1}) was adjusted to initial values ranging from 2 to 12. The suspensions were agitated 48 h at room temperature, and the variation of pH ($\Delta pH = pH_{final} - pH_{initial}$) was measured and plotted versus the initial pH. The pH_{PZC} is identified as the point at which the variation of pH is equal to 0, as shown in Fig. 8. The pH_{pzc} of nanocomposite was found to be at a pH = 6.8.

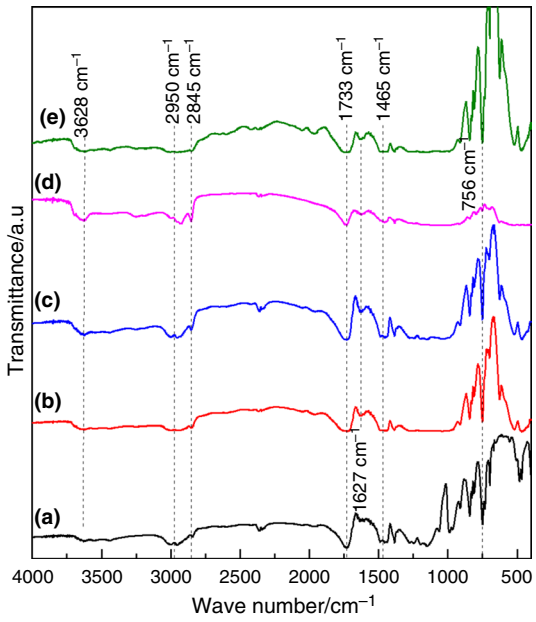

Fig. 7 FTIR spectra of PMMA/OMMT nanocomposites with various OMMT loading: **a** 0%, **b** 1%, **c** 3%, **d** 5% and **e** 7%

Dye adsorption results

Effect of pH

The surface charge of the adsorbent can be affected by the pH of the solution, which creates the essential force between the adsorbent and the adsorbate [57].

Figure 9 shows the pH effect on the adsorption of the azo dye onto nanocomposite sample.

As can be seen from figure, the adsorption capacity remains stable throughout the pH range (2–12) indicating that the adsorption is independent of pH.

The similar results were reported by Kırans et al. [58] for studying the adsorption of an anionic dye onto organoclay. Hence, we conclude that the pH has no effect on the adsorption capacity of organoclay/PMMA nanocomposite. This behavior was explained by electrostatic interactions between the negative charges of the SO_3^- group of the dye and the positive charges of the ammonium groups of the surfactant containing in nanocomposite adsorbent [58].

Effect of contacting time and kinetics modeling

Equilibrium contacting time is a crucial parameter in economic wastewater treatment systems [59]. The adsorption kinetics of dye on PMMA/OMMT nanocomposite with initial concentrations of 25, 50 and 100 mg L^{-1} at 293 K was examined and the results are illustrated in Fig. 10a. The equilibrium time of adsorption was reached very rapidly within 20 min.

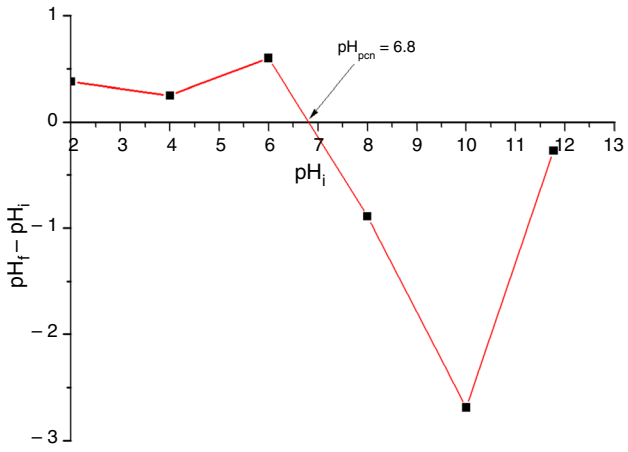

Fig.8 Isoelectric point (pH_{pcn}) determination for PMMA/OMMT nanocomposite

The pseudo-1st order kinetic model, pseudo-2nd order kinetic model and intraparticle diffusion mode were used to examine the adsorption kinetics.

Pseudo-1st order kinetic model Eq. (5):

$$\ln\left(q_e - q_t\right) = \ln q_e - k_1 t \tag{5}$$

where q_t and q_e are, respectively, the adsorption amount at instant t and at equilibrium (mg g^{-1}), t is the contacting time (min) and k_1 is the kinetic coefficient (min^{-1});

(ii) Pseudo-2nd order kinetic model Eq. (6):

$$t/q_t = 1/k_2 q_e^2 + t/q_e \tag{6}$$

where $k_2$is the kinetic coefficient (g mg^{-1} min^{-1}).

(iii) Intraparticle diffusion model Eq. (7):

$$q_t = K_d \cdot t^{0.5} + C \tag{7}$$

According to the experimental results, pseudo-first order kinetic model, pseudo-second order kinetic model and intraparticle diffusion mode has been compared to examine the adsorption rate, and the results are represented in Table 2. We have found that the pseudo-second order kinetic is the appropriate model for describing the adsorption and with R^2 near to 1; the model is in accordance with the experimental data from 0 to 240 min. The theoretical adsorption capacities of 8 mg g^{-1} ($C_0 = 25$ mg L^{-1}), 28.57 mg/g ($C_0 = 50$ mg L^{-1}) and 100 mg g^{-1} ($C_0 = 100$ mg L^{-1}) were, respectively, near to the experimental values of 9.52, 32.38 and 101.75 mg g^{-1}. The pseudo-second order kinetics modeling curves are represented in Fig. 10(b).

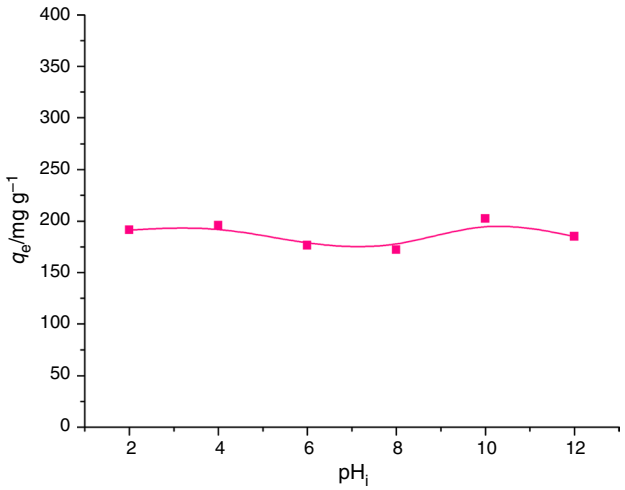

Fig. 9 Effect of pH on adsorption of Nylosan Red by PMMA/OMMT nanocomposite

Effect of initial azo dye concentration and adsorption isotherm

The adsorption capacity (q_e) and adsorption efficiency percentage (R (%)) of the azo dye at the equilibrium onto adsorbent (PMMA/OMMT) versus initial dye concentration was plotted (Fig. 11). It can be seen that at low initial dye concentrations (≤ 100 mg L^{-1}), there is a high adsorption efficiency

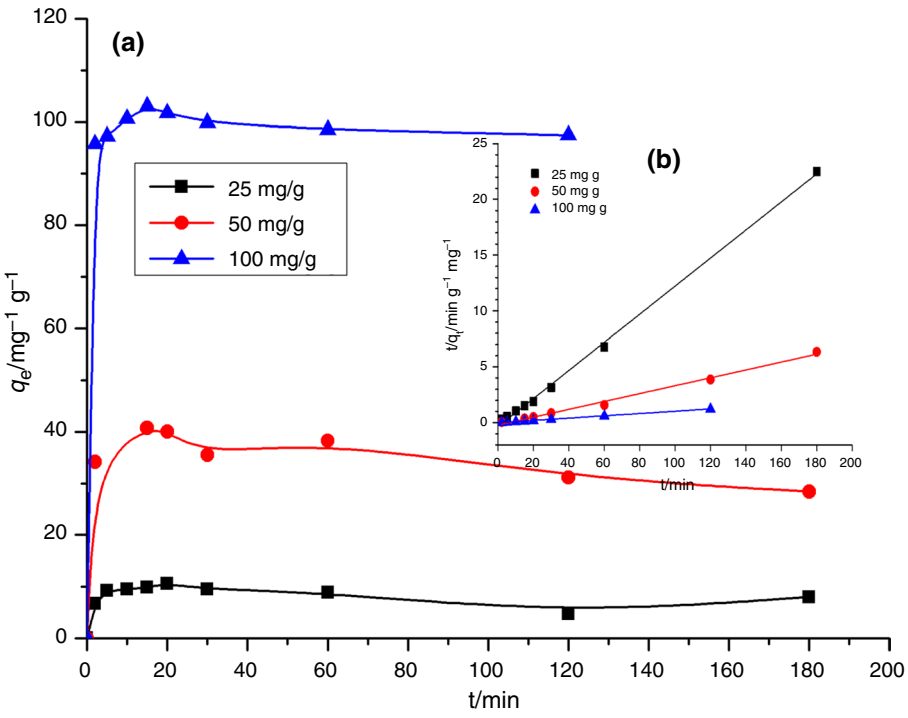

Fig. 10 Adsorption kinetic of Nylosan Red dye onto PMMA/OMMT nanocomposite (**a**), and pseudo-second-order kinetics modeling (**b**)

(85%), and it was unchanged in this range of concentrations. The adsorption capacity (q_e) is strongly increased to 98 mg/g with increasing in initial azo dye concentration at low concentrations. However, the adsorption efficiency is decreased gradually from 85 to 70% by increasing of initial dye concentration from 100 to 300 mg L^{-1}, and the adsorption capacity (q_e)was still increased to $q_e = 270$ mg g^{-1}. In the last range concentration (300–600 mg L^{-1}), the adsorption efficiency percentage is strongly decreased from 70 to 36%. Moreover, the adsorption capacity (q_e) is slowly increased from 270 to 280 mg g^{-1} with increasing initial dye concentration. Before plotting of adsorption isotherm, the type (*L*) is the appropriate model. Because in this isotherm, the adsorption is high in low initial concentrations of adsorbate and become less in high concentration until saturation of adsorption sites. The isotherm adsorption of Nylosan Red dye onto PMMA/OMMT 7% nanocomposite is represented in Fig. 12.

The adsorption isotherms at equilibrium can be graphically depicted by plotting of solid phase amounts versus liquid phase concentrations.

In order to explain the interactions between the adsorbent and adsorbate, different theories concerning the adsorption equilibrium isotherms have been proposed, single component adsorption isotherm equations have been examined in the present paper, namely Langmuir (L), Freundlich (F) and Dubinin–Radushkevich (D–R). The linearized form of these isotherms was represented by the following equations:

The Langmuir isotherm is given by the Eq. (8), which implies that adsorption takes place at homogenous sites located in the adsorbent surface Eq. (8) [60]:

$$C_e/q_e = 1/kq_m + \left(1/q_m\right)C_e \tag{8}$$

where q_e is the quantity of azo dye adsorbed per gram of adsorbent (mg g^{-1}). C_e is the equilibrium remaining concentration of azo dye in solution (mg L^{-1}). q_m is the maximal adsorption capacity (mg g^{-1}), which corresponds to total monolayer coverage and k is a constant related to the energy or net enthalpy.

Equation (9) [60] gives the Freundlich isotherm, which is used to describe adsorption tests occurring on heterogeneous adsorbent surfaces:

Table 2 Kinetic constants for Nylosan Red dye adsorption onto PMMA/OMMT 7% nanocomposite

	Pseudo first-order				Pseudo-second-order			Intraparticle diffusion model		
	$q_{e\ (exp)}$/mg g^{-1}	q_e (The)/mg g^{-1}	k_1/min^{-1}	R^2	$q_{e\ (The)}$/mg g^{-1}	K_2/g mg^{-1} min^{-1}	R^2	K_d/mg g^{-1} $t^{0.5}$	C/mg g^{-1}	R^2
25 mg/L	9.52	4.1	0.143	0.515	8	0.044	0.998	1.09	5.90	0.779
50 mg/L	32.38	3.90	0.012	0.440	28.57	0.005	0.991	7.62	24.89	0.746
100 mg/L	101.75	10.50	0.216	0.905	100	0.025	0.999	2.34	92.56	0.848

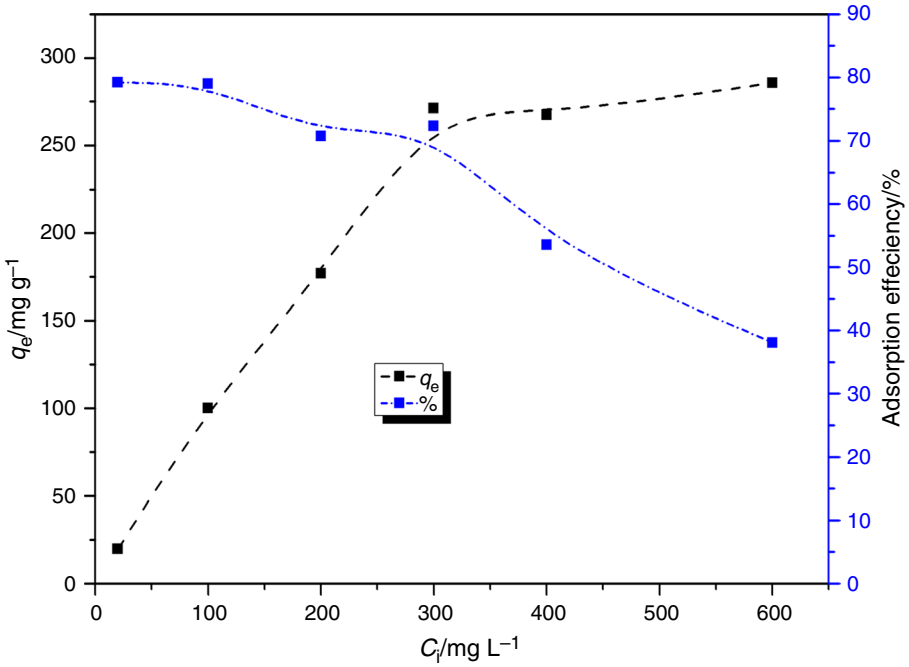

Fig. 11 Influence of initial Nylosan Red dye concentration on the adsorption capacity and the percentage dye removal by PMMA/OMMT 7% nanocomposite

$$\mathrm{Log}q_e = \mathrm{Log}k_f + (1/n)\mathrm{Log}C_e \quad (9)$$

where K_f and n are the Freundlich constants associated with adsorption capacity and adsorption intensity that can be determined, respectively, from the intercept and slope of log q_e versus LogC_e plot.

The Dubinin–Radushkevich isotherm model given by the Eq. (10) [60] does not assumes a constant sorption potential. It can be noted that it is more general than the Langmuir model:

$$\begin{aligned} \ln q_e &= \ln q_m - B\varepsilon^2 \\ \varepsilon &= RT \ln\left(1 + 1/C_e\right) \end{aligned} \quad (10)$$

where B is a constant associated with adsorption energy (mol J^{-1}), q_m is the theoretical adsorption capacity (mg g^{-1}), and ε is the Polanyi potential. B and q_m may be calculated, respectively, from the slope and intercept of lnq_e versus ε^2.

According to the obtained results (Fig. 13 and Table 3), the best experimental data fit for azo dye was obtained by the Langmuir isotherm model (high R^2 value compared to Freundlich and Dubinin–Radushkevich isotherms models) with maximum monolayer adsorption capacity of 309.6 mg g^{-1} (0.53 mmol g^{-1}).

Thermodynamic study

The adsorption thermodynamic is investigated for nanocomposite sample.

The adsorption capacity of azo dye at different temperature (25 °C, 35 °C and 45 °C) were plotted and represented in Fig. 14a. It is clearly noticed that the adsorption capacities of azo dye increases (22–34 mg g^{-1}) with increasing of temperature within the temperature range (25–45 °C). It means that the adsorption process was endothermic. From these results, thermodynamic parameters including the variation in free energy (ΔG°) with three temperatures, enthalpy (ΔH°) and entropy (ΔS°) were used to describe thermodynamic behavior of the adsorption of azo dye onto nanocomposite. To calculate the thermodynamic parameters, we used the following equation to determine the Gibbs free energy at three temperatures:

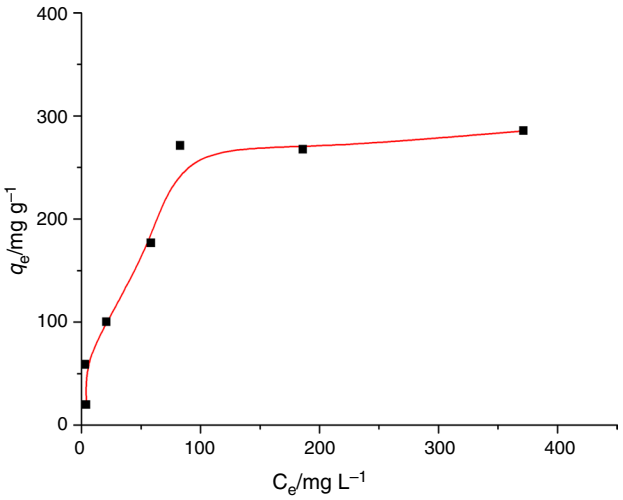

Fig. 12 Adsorption isotherm of Nylosan Red dye onto PMMA/OMMT nanocomposite

$$\Delta G^\circ = -RT \ln K_d \quad (11)$$

where R is the constant of perfect gas ($R = 8.314$ J mol^{-1} K^{-1}), T is the temperature of adsorbate–adsorbent suspension (K), K_d is the distribution constant, can be expressed as: $K_d = q_e/C_e$, q_e and C_e are the adsorption capacity (mg g^{-1}) and remaining concentration of dye solution (mg L^{-1}), respectively.

The relationship between $\Delta G°$, $\Delta H°$ and $\Delta S°$ is given by:

$$\Delta G^\circ = \Delta H^\circ - T\Delta S^\circ \quad (12)$$

Substituting Eq. 11 into 12, we obtained the well-known vant' Hoff equation:

$$\mathrm{Ln}\, K_d = -\Delta H°/RT + \Delta S°/R \quad (13)$$

The enthalpy (ΔH°) and entropy (ΔS°) of adsorption were estimated from the slope and intercept of the plot of ln K_d versus $1/T$, respectively. (slope $= -\Delta H°/R$ and intercept $= \Delta S°/R$). The curve Ln $K_d = f(1/T)$ and calculated thermodynamic parameters are illustrated in Fig. 14b and Table 4, respectively. The positive value of ΔH°, 33.2 kJ mol^{-1}, indicates an endothermic adsorption process for azo dye, the positive value of ΔS°, 106.5 J mol^{-1} K^{-1}, suggests an increase in the randomness at the solid/solution interface during the adsorption reaction. The results revealed also that as the temperature was increased; negative values of (ΔG) were found to increase, which indicate that the adsorption is energetic and more favorable.

Additionally, the ΔH value can be used to indicate the nature of adsorption, physisorption (5–50 kJ mol^{-1}) or chemisorption (50–80 kJ mol^{-1}) [38]. Therefore, adsorption of azo dye onto nanocomposite sample is physical adsorption dominated by van der Waals forces between nanocomposite molecules and azo dye molecules. The adsorption rate in this nature was also high. Therefore, increasing the temperature is beneficial to improve the adsorption of azo dye onto nanocomposite.

Reusability of nanocomposite adsorbent

We have thoroughly investigated the reusability of the prepared adsorbent. To assess its practical applicability,

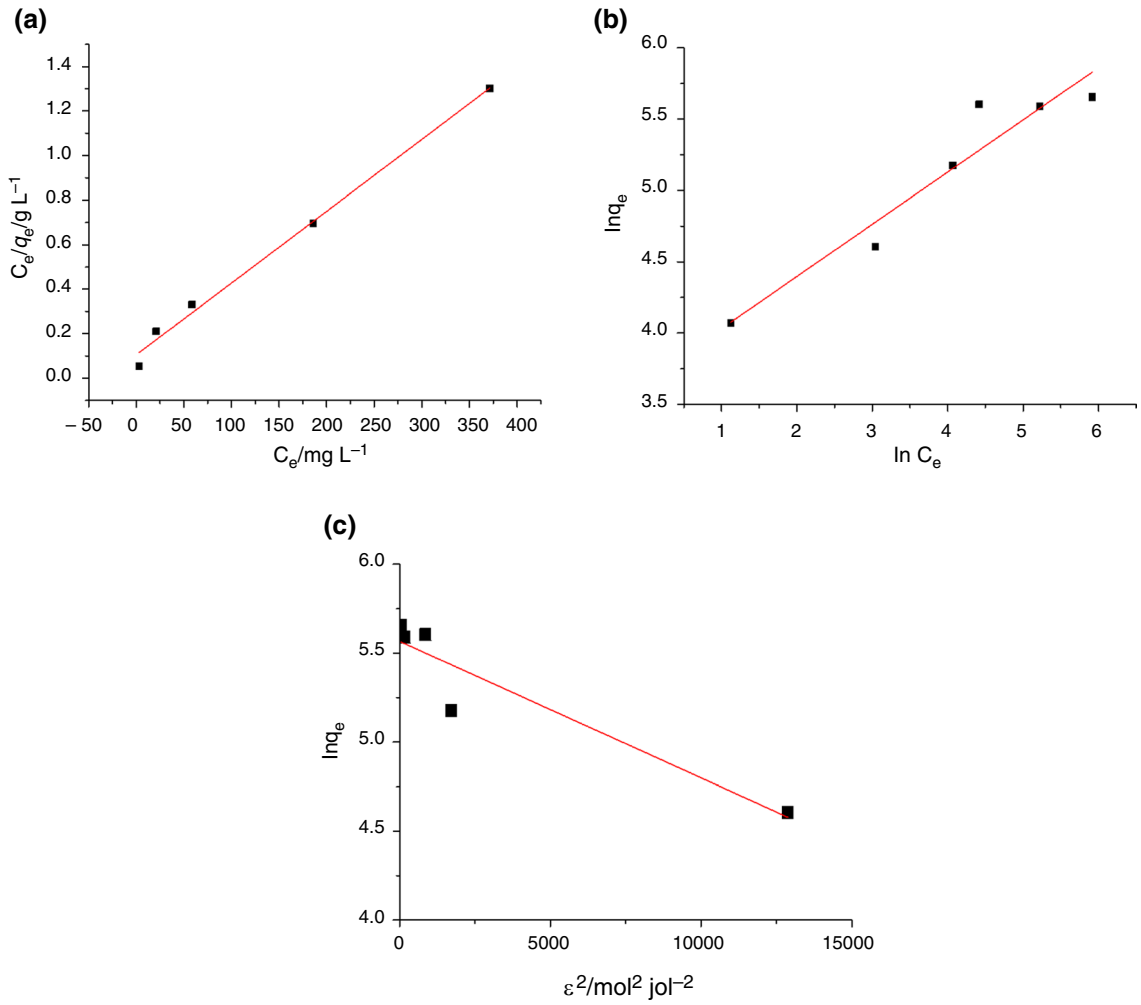

Fig. 13 Isotherms modeling of Langmuir (**a**), Freundlich **b**, **c** Dubinin–Radushkevich model for adsorption of Nylosan Red dye onto PMMA/OMMT nanocomposite

Table 3 Langmuir, Freundlich and D–R constants for the adsorption of Nylosan Red dye on PMMA/OMMT 7% nanocomposite

Langmuir			Freundlich			Dubinin–Radushkevich		
q_m/mg g^{-1}	K_L/L mg^{-1}	R^2	K_f	n	R^2	q_m/mg g^{-1}	B°10^{-5}/mol J^{-1}	R^2
309.6	0.031	0.997	39.16	2.735	0.961	261.25	7.66	0.852

we conducted three consecutive cycles of azo adsorption using the nanocomposite sample, as illustrated in Fig. 15. The results of our study demonstrate that the adsorption capacity of the nanocomposite sample experienced only a marginal decrease of 12% after three cycles of utilizing the adsorbent. This minor reduction is deemed insignificant and underscores the remarkable stability and reusability of the nanocomposite in the context of azo dye adsorption.

Comparison of the current study with earlier studies

For comparison with the PMMA/OMMT nanocomposite, numerous adsorbents for NR azo dye have been reported and listed in Table 5. The nanocomposite sample has higher adsorption capacity than the adsorbents mentioned in the earlier reported studies. This study showed that the

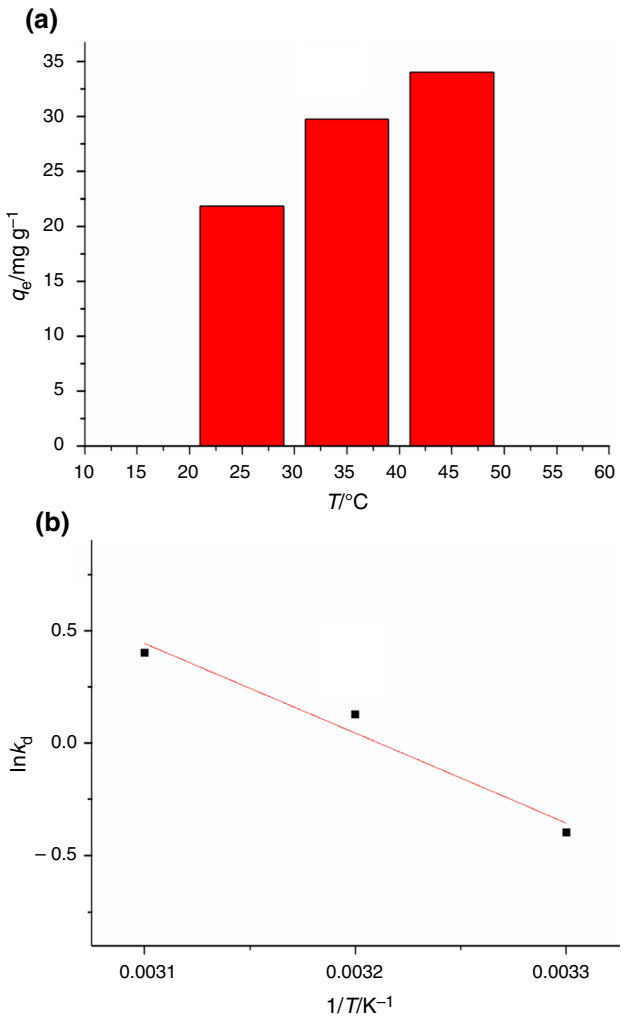

Fig. 14 Effect of temperature on adsorption capacity of nanocomposite sample (**a**) and ln K_d versus 1/T graph employed in the evaluation of thermodynamic parameters (**b**)

Table 4 Thermodynamic parameters of azo dye adsorption on nanocomposite

T/K	ΔG°/kJ mol^{-1}	ΔH°/kJ mol^{-1}	ΔS°/J mol K^{-1}
293.15	0.98	33.2	106.5
303.15	− 0.32		
313.15	− 1.06		

prepared nanocomposite is able to remove high amounts of azo dye and can be employed when very polluted waters should be treated.

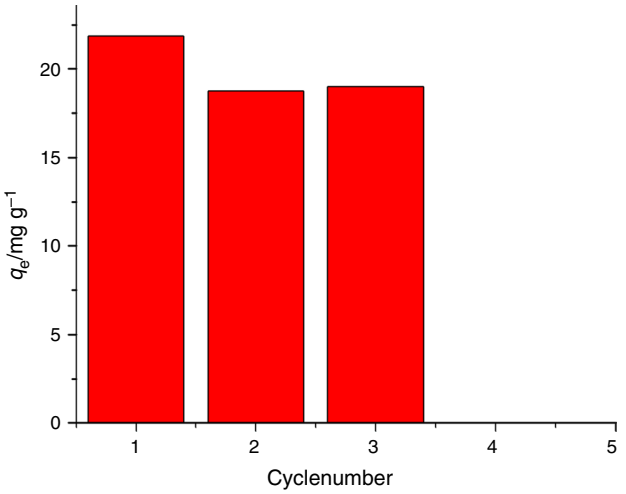

Fig. 15 Reusability performance of nanocomposite for the adsorptive removal of azo dye (C_0: 50 mg L^{-1}; T: 25 °C; t = 2 h)

Table 5 Comparison of adsorption capacity of Nylosan Red dye on to various adsorbents

Adsorbents	Q_{max}/mg g^{-1}	References
Cynara cardunculus (CARD)	83.33	[37]
Eucalyptus globulus (EUCA)	83.33	[37]
Prunus cerasifera (PRUN)	76.92	[37]
Activated carbon (CGAC120)	116	[34]
HS	25.18	[40]
Fractionated sodium montmorillonite	201	[39]
PMMA/OMT nanocomposite	309.6	This study

Conclusions

In this study, the synthesis and comprehensive characterization of exfoliated PMMA/OMMT nanocomposites were undertaken, focusing on the morphological, structural, thermal, and adsorption properties of the resulting materials. SEM analysis revealed excellent and homogeneous dispersion of OMMT microsheets in the PMMA matrix. XRD patterns demonstrated an increase in d-value, supporting effective intercalation of octadecylammonium within montmorillonite layers. TEM analysis provided complementary insights, particularly for PMMA/OMMT 1% and PMMA-OMMT7%, revealing a mixed morphology of intercalated and exfoliated structures. The TEM images of PMMA/OMMT 1% demonstrated well-dispersed and disoriented clay platelets, while PMMA/OMMT 7% exhibited clear exfoliated clay platelets. Thermal analyses (TG and DTA) revealed that the thermal stability of PMMA/OMMT nanocomposites was significantly improved (approximately

34 °C higher) in comparison with pure PMMA. The glass transition temperature (T_g) of pure PMMA increases following the incorporation of organomontmorillonite into the polymer matrix, exhibiting an elevation of approximately 21 °C. FTIR spectra confirmed successful OMMT incorporation into the polymer matrix, with shifts in specific peaks indicating interactions between PMMA and OMMT. The adsorption study revealed efficient removal of azo dye, with stable performance over three usage cycles, showcasing the remarkable reusability of the PMMA/OMMT nanocomposite. Furthermore, the thermodynamic analysis suggested an endothermic and energetically favorable adsorption process, dominated by physical adsorption forces. The nanocomposite displayed high adsorption capacities, outperforming various reported adsorbents for azo dye. This study establishes PMMA/OMMT nanocomposites as promising materials for efficient and reusable removal of azo dyes from polluted waters.

Author contributions ST was contributed to elaboration, characterization, methodology, data curation, investigation, writing—review and editing. SH was contributed to methodology, data curation, writing—review and editing. NL was contributed to elaboration, characterization, data curation. KB was contributed to characterization. HBR was contributed to characterization.

References

1. Ali U, Karim KJBA, Buang NA. A review of the properties and applications of poly (methyl methacrylate) (PMMA). Polym Rev. 2015;55:678–705.
2. Nikolaidis AK, Achilias DS, Karayannidis GP. Effect of the type of organic modifier on the polymerization kinetics and the properties of poly(methyl methacrylate)/organomodified montmorillonite nanocomposites. Eur Polym J. 2012;48:240–51. https://doi.org/10.1016/j.eurpolymj.2011.11.004.
3. Rajabi M, Mahanpoor K, Moradi O. Preparation of PMMA/GO and PMMA/GO-Fe_3O_4 nanocomposites for malachite green dye adsorption: kinetic and thermodynamic studies. Compos Part B. 2019;167:544–55. https://doi.org/10.1016/j.compositesb.2019.03.030.
4. Barwood MJ, Breen C, Clegg F, Hammond CL. The effect of organoclay addition on the properties of an acrylate based, thermally activated shape memory polymer. Appl Clay Sci. 2014;102:41–50. https://doi.org/10.1016/j.clay.2014.10.010.
5. Cui L, Tarte NH, Woo SI. Effects of modified clay on the morphology and properties of PMMA/clay nanocomposites synthesized by in situ polymerization. Macromolecules. 2008;41:4268–74.
6. Wang X, Su Q, Hu Y, Wang C, Zheng J. Structure and thermal stability of PMMA/MMT nanocomposites as denture base material. J Therm Anal Calorim. 2014;115:1143–51.
7. Melouki A, Terchi S, Ouali D, Bounab A. Preparation of new copolymer (polystyrene/TMSPM grafted on DDA-fractionated algerian montmorillonite) hybrid organoclay by radical copolymerization: structural study, thermal stability and hydrophobicity area. J Therm Anal Calorim. 2021. https://doi.org/10.1007/s10973-021-10935-8.
8. Zhao Q, Samulski ET. In situ polymerization of poly(methyl methacrylate)/clay nanocomposites in supercritical carbon dioxide. Macromolecules. 2005;38:7967–71.
9. Hegyesi N, Pongrácz S, Vad RT, Pukánszky B. Coupling of PMMA to the surface of a layered silicate by intercalative polymerization: processes, structure and properties. Colloids Surf A Physicochem Eng Asp. 2020;601:124979. https://doi.org/10.1016/j.colsurfa.2020.124979.
10. Prado BR, Bartoli JR. Synthesis and characterization of PMMA and organic modified montmorilonites nanocomposites via in situ polymerization assisted by sonication. Appl Clay Sci. 2018;160:132–43. https://doi.org/10.1016/j.clay.2018.02.035.
11. Qin X, Wu Y, Wang K, Tan H, Nie J. In-situ synthesis of exfoliated nanocomposites by photopolymerization using a novel montmorillonite-anchored initiator. Appl Clay Sci. 2009;45:133–8. https://doi.org/10.1016/j.clay.2009.04.014.
12. Li P, Khan MA, Xia M, Lei W, Zhu S, Wang F. Efficient preparation and molecular dynamic (MD) simulations of Gemini surfactant modified layered montmorillonite to potentially remove emerging organic contaminants from wastewater. Ceram Int. 2019;45:10782–91. https://doi.org/10.1016/j.ceramint.2019.02.152.
13. Andrade M, Nelson S, Larocca M, Antonio L. Highly thermal stable organoclays of ionic liquids and silane organic modifiers and effect of montmorillonite source. J Therm Anal Calorim. 2016;126:499–509.
14. Youssef AM, Malhat FM, Abdel Hakim AA, Dekany I. Synthesis and utilization of poly (methylmethacrylate) nanocomposites based on modified montmorillonite. Arab J Chem. 2017;10:631–42. https://doi.org/10.1016/j.arabjc.2015.02.017.
15. Valandro SR, Lombardo PC, Poli AL, Horn MA, Neumann MG, Cavalheiro CCS. Thermal properties of poly (methyl methacrylate)/organomodified montmorillonite nanocomposites obtained by in situ photopolymerization. Mater Res. 2014;17:265–70.
16. Holkar CR, Jadhav AJ, Pinjari DV, Mahamuni NM, Pandit AB. A critical review on textile wastewater treatments: possible approaches. J Environ Manage. 2016;182:351–66. https://doi.org/10.1016/j.jenvman.2016.07.090.
17. Shenouda SS, Hussien MSA, Parditka B, Csík A, Takats V, Erdélyi Z. Novel amorphous Al-rich Al_2O_3 ultra-thin films as active photocatalysts for water treatment from some textile dyes. Ceram Int. 2020;46:7922–9. https://doi.org/10.1016/j.ceramint.2019.12.012.
18. Kausar A, Iqbal M, Javed A, Aftab K, Nazli ZIH, Bhatti HN, et al. Dyes adsorption using clay and modified clay: a review. J Mol Liq. 2018;256:395–407. https://doi.org/10.1016/j.molliq.2018.02.034.
19. Li N, Yang B, Xu L, Xu G, Sun W, Yu S. Simple synthesis of Cu_2O/Na-bentonite composites and their excellent photocatalytic properties in treating methyl orange solution. Ceram Int. 2016;42:5979–84. https://doi.org/10.1016/j.ceramint.2015.12.145.
20. Samchetshabam G, Hussan A, Choudhury TG, Gita S. Impact of textile dyes waste on aquatic environments and its treatment wastewater management view project tribal sub plan view project. Environ Ecol. 2017;35:2349–53.
21. Sivaraj D, Vijayalakshmi K, Srinivasan M, Ramasamy P. Graphene oxide reinforced bismuth titanate for photocatalytic degradation of azo dye (DB15) prepared by hydrothermal method. Ceram Int. 2021;47:25074–80. https://doi.org/10.1016/j.ceramint.2021.05.238.
22. Ben Dassi R, Chamam B, Méricq JP, Heran M, Faur C, El Mir L, et al. Pb doped ZnO nanoparticles for the sorption of reactive black 5 textile azo dye. Water Sci Technol. 2020;82:2576–91.
23. Heibati B, Rodriguez-Couto S, Amrane A, Rafatullah M, Hawari A, Al-Ghouti MA. Uptake of Reactive Black 5 by pumice and walnut activated carbon: chemistry and adsorption mechanisms.

J Ind Eng Chem. 2014;20:2939–47. https://doi.org/10.1016/j.jiec.2013.10.063.
24. Raj S, Singh H, Bhattacharya J. Treatment of textile industry wastewater based on coagulation-flocculation aided sedimentation followed by adsorption: process studies in an industrial ecology concept. Sci Total Environ. 2023;857:159464. https://doi.org/10.1016/j.scitotenv.2022.159464.
25. Khemila B, Merzouk B, Chouder A, Zidelkhir R, Leclerc J. Removal of a textile dye using photovoltaic electrocoagulation. Sustain Chem Pharm. 2018;7:27–35. https://doi.org/10.1016/j.scp.2017.11.004.
26. Belayachi-Haddad A, Benderdouche N, Bestani B, Duclaux L. Synthetic textile wastewater treatment: removal of Nylosan (N-2RBL) dye by electrocoagulation. Desalin Water Treat. 2017;63:78–86.
27. Raza N, Raza W, Gul H, Kim KH. ZnO–ZnTe hierarchical superstructures as solar-light-activated photocatalysts for azo dye removal. Environ Res. 2021;194:110499. https://doi.org/10.1016/j.envres.2020.110499.
28. Chakraborty A, Ruzimuradov O, Gupta RK, Cho J, Prakash J. TiO_2 nanoflower photocatalysts: synthesis, modifications and applications in wastewater treatment for removal of emerging organic pollutants. Environ Res. 2022;212:113550. https://doi.org/10.1016/j.envres.2022.113550.
29. Chankhanittha T, Komchoo N, Senasu T, Piriyanon J, Youngme S, Hemavibool K, et al. Silver decorated ZnO photocatalyst for effective removal of reactive red azo dye and ofloxacin antibiotic under solar light irradiation. Colloids Surf A Physicochem Eng Asp. 2021;626:127034. https://doi.org/10.1016/j.colsurfa.2021.127034.
30. Ghaemi N, Madaeni SS, Daraei P, Rajabi H, Shojaeimehr T, Rahimpour F, et al. PES mixed matrix nanofiltration membrane embedded with polymer wrapped MWCNT: fabrication and performance optimization in dye removal by RSM. J Hazard Mater. 2015;298:111–21. https://doi.org/10.1016/j.jhazmat.2015.05.018.
31. Ouachtak H, El Guerdaoui A, Haounati R, Akhouairi S, El Haouti R, Hafid N, et al. Highly efficient and fast batch adsorption of orange G dye from polluted water using superb organo-montmorillonite: experimental study and molecular dynamics investigation. J Mol Liq. 2021;335: 116560.
32. Joshiba GJ, Kumar PS, Rangasamy G, Ngueagni PT, Pooja G, Balji GB, et al. Iron doped activated carbon for effective removal of tartrazine and methylene Blue dye from the aquatic systems: kinetics, isotherms, thermodynamics and desorption studies. Environ Res. 2022;215:114317. https://doi.org/10.1016/j.envres.2022.114317.
33. Ullah F, Ji G, Irfan M, Gao Y, Shafiq F, Sun Y, et al. Adsorption performance and mechanism of cationic and anionic dyes by KOH activated biochar derived from medical waste pyrolysis. Environ Pollut. 2022;314:120271. https://doi.org/10.1016/j.envpol.2022.120271.
34. Reffas A, Bernardet V, David B, Reinert L, Lehocine MB, Dubois M, et al. Carbons prepared from coffee grounds by H_3PO_4 activation: characterization and adsorption of methylene Blue and Nylosan Red N-2RBL. J Hazard Mater. 2010;175:779–88.
35. Ngeno EC, Mbuci KE, Necibi MC, Shikuku VO, Olisah C, Ongulu R, et al. Sustainable re-utilization of waste materials as adsorbents for water and wastewater treatment in Africa: recent studies, research gaps, and way forward for emerging economies. Environ Adv. 2022;9:100282.
36. Tee GT, Gok XY, Yong WF. Adsorption of pollutants in wastewater via biosorbents, nanoparticles and magnetic biosorbents: a review. Environ Res. 2022;212:113248. https://doi.org/10.1016/j.envres.2022.113248.
37. Ouldmoumna A, Benderdouche N, Reinert L, Bestani B, Duclaux L. Adsorption of red nylosane solution on natural materials. Desalin Water Treat. 2017;65:304–12.
38. Tabrizi SH, Tanhaei B, Ayati A, Ranjbari S. Substantial improvement in the adsorption behavior of montmorillonite toward Tartrazine through hexadecylamine impregnation. Environ Res. 2022;204:111965. https://doi.org/10.1016/j.envres.2021.111965.
39. Terchi S, Ladjal N, Zidelkheir B, Bachari K. Adsorption performance of anionic textile dye (Nylosan red n-2rbl) onto raw, sodic and fractionated sodic inorganic clay material. Rev Roum Chim. 2020;65:869–84.
40. Karakuş S, Taşaltın N, Taşaltın C, Kilislioğlu A. Comparative study on ultrasonic assisted adsorption of Basic Blue 3, Basic Yellow 28 and Acid Red 336 dyes onto hydromagnesite stromatolite: kinetic, isotherm and error analysis. Surf Interfaces. 2020;20:100528. https://doi.org/10.1016/j.surfin.2020.100528.
41. Zhu Y, Cui Y, Peng Y, Dai R, Chen H, Wang Y. Preparation of CTAB intercalated bentonite for ultrafast adsorption of anionic dyes and mechanism study. Colloids Surf A Physicochem Eng Asp. 2023;658:130705. https://doi.org/10.1016/j.colsurfa.2022.130705.
42. Mallakpour S, Hatami M. An effective, low-cost and recyclable bio-adsorbent having amino acid intercalated LDH@Fe_3O_4/PVA magnetic nanocomposites for removal of methyl orange from aqueous solution. Appl Clay Sci. 2019;174:127–37. https://doi.org/10.1016/j.clay.2019.03.026.
43. Minisy IM, Salahuddin NA, Ayad MM. Adsorption of methylene blue onto chitosan–montmorillonite/polyaniline nanocomposite. Appl Clay Sci. 2021;203:105993. https://doi.org/10.1016/j.clay.2021.105993.
44. Ulu A, Alpaslan M, Gultek A, Ates B. Eco-friendly chitosan/κ-carrageenan membranes reinforced with activated bentonite for adsorption of methylene blue. Mater Chem Phys. 2022;278:125611.
45. Ladjal N, Zidelkheir B, Terchi S. Influence of octadecylammonium, *N*,*N*-dimethylhexadecylammonium, and 1-hexadecyltrimethylammonium chloride upon the fractionated montmorillonite. J Therm Anal Calorim. 2018;134:881–8. https://doi.org/10.1007/s10973-018-7237-4.
46. Fu X, Qutubuddin S. Polymer-clay nanocomposites: exfoliation of organophilic montmorillonite nanolayers in polystyrene. Polymer (Guildf). 2001;42:807–13.
47. Kowalczyk K, Spychaj T, Ubowska A, Schmidt B. Industrially applicable methods of poly(methyl methacrylate)/organophilic montmorillonite nanocomposites preparation: processes and cast materials characterization. Appl Clay Sci. 2014;97–98:96–103. https://doi.org/10.1016/j.clay.2014.05.011.
48. Valandro SR, Poli AL, Neumann MG, Schmitt CC. Organomontmorillonite/poly(methyl methacrylate) nanocomposites prepared by in situ photopolymerization. Effect of the organoclay on the photooxidative degradation. Appl Clay Sci. 2013;85:19–24. https://doi.org/10.1016/j.clay.2013.08.050.
49. Tsai TY, Lin MJ, Chuang YC, Chou PC. Effects of modified clay on the morphology and thermal stability of PMMA/clay nanocomposites. Mater Chem Phys. 2013;138:230–7. https://doi.org/10.1016/j.matchemphys.2012.11.051.
50. Morgan AB, Gilman JW. Characterization of polymer-layered silicate (clay) nanocomposites by transmission electron microscopy and X-ray diffraction: a comparative study. J Appl Polym Sci. 2002;87:1329–38.
51. Hirata T, Kashiwagi T, Brown JE. Thermal and oxidative degradation of poly(methyl methacrylate): weight loss. Macromolecules. 1985;18:1410–8.
52. McNeill IC. A study of the thermal degradation of methyl methacrylate polymers and copolymers by thermal volatilization analysis. Eur Polym J. 1968;4:21–30.

53. Temuujin J, Jadambaa T, Burmaa G, Erdenechimeg S, Amarsanaa J, MacKenzie KJD. Characterisation of acid activated montmorillonite clay from Tuulant (Mongolia). Ceram Int. 2004;30:251–5.
54. Mishra AK, Allauddin S, Narayan R, Aminabhavi TM, Raju KVSN. Characterization of surface-modified montmorillonite nanocomposites. Ceram Int. 2012;38:929–34. https://doi.org/10.1016/j.ceramint.2011.08.012.
55. Liu Y, Lee JY, Hong L. Synthesis, characterization and electrochemical properties of poly(methyl methacrylate)-grafted-poly(vinylidene fluoride-hexafluoropropylene) gel electrolytes. Solid State Ion. 2002;150:317–26.
56. Kuo SW, Kao HC, Chang FC. Thermal behavior and specific interaction in high glass transition temperature PMMA copolymer. Polymer (Guildf). 2003;44:6873–82.
57. Ahsani-Namin Z, Norouzbeigi R, Shayesteh H. Green mediated combustion synthesis of copper zinc oxide using *Eryngium planum* leaf extract as a natural green fuel: excellent adsorption capacity towards Congo red dye. Ceram Int. 2022;48:20961–73. https://doi.org/10.1016/j.ceramint.2022.04.090.
58. Kiranşan M, Soltani RDC, Hassani A, Karaca S, Khataee A. Preparation of cetyltrimethylammonium bromide modified montmorillonite nanomaterial for adsorption of a textile dye. J Taiwan Inst Chem Eng. 2014;45:2565–77.
59. Safarzadeh H, Peighambardoust SJ, Mousavi SH, Foroutan R, Mohammadi R, Peighambardoust SH. Adsorption ability evaluation of the poly(methacrylic acid-co-acrylamide)/cloisite 30B nanocomposite hydrogel as a new adsorbent for cationic dye removal. Environ Res. 2022;212:113349. https://doi.org/10.1016/j.envres.2022.113349.
60. da Silva MA, Dias DDS, Capela JMV, Fertonani IAP, Ribeiro CA. Biochar from Pine cone (strobilus of *Pinus elliottii*) by torrefaction process: evaluation of the adsorptive and energy capacity. J Therm Anal Calorim. 2023;148:12321–33. https://doi.org/10.1007/s10973-023-12461-1.